Article

Design, Synthesis, and Evaluation of a Lanthanide Chelating Protein Probe: CLaNP-5 Yields Predictable Paramagnetic Effects Independent of Environment

Peter H. J. Keizers, Athanasios Saragliadis, Yoshitaka Hiruma, Mark Overhand, and Marcellus Ubbink

J. Am. Chem. Soc., **2008**, 130 (44), 14802-14812 • DOI: 10.1021/ja8054832 • Publication Date (Web): 01 October 2008

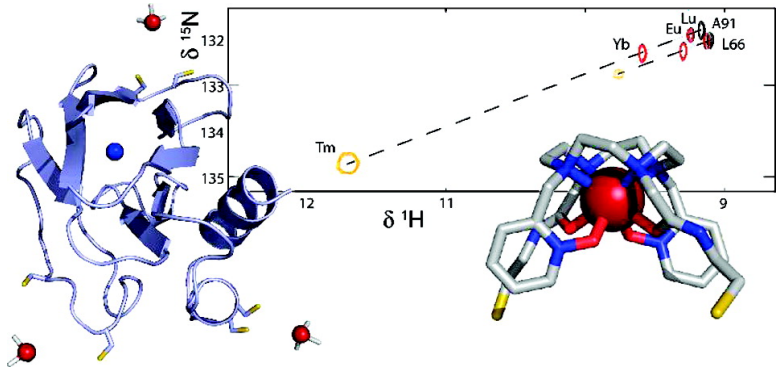

More About This Article

Additional resources and features associated with this article are available within the HTML version:

- Supporting Information
- Links to the 1 articles that cite this article, as of the time of this article download
- Access to high resolution figures
- Links to articles and content related to this article
- Copyright permission to reproduce figures and/or text from this article

View the Full Text HTML

J|A|C|S
ARTICLES

Published on Web 10/01/2008

Design, Synthesis, and Evaluation of a Lanthanide Chelating Protein Probe: CLaNP-5 Yields Predictable Paramagnetic Effects Independent of Environment

Peter H. J. Keizers, Athanasios Saragliadis, Yoshitaka Hiruma, Mark Overhand, and Marcellus Ubbink*

Leiden Institute of Chemistry, Gorlaeus Laboratories, Leiden University, Post Office Box 9502, 2300 RA Leiden, The Netherlands

Received July 15, 2008; E-mail: m.ubbink@chem.leidenuniv.nl

Abstract: Immobilized lanthanide ions offer the opportunity to refine structures of proteins and the complexes they form by using restraints obtained from paramagnetic NMR experiments. We report the design, synthesis, and spectroscopic evaluation of the lanthanide chelator, Caged Lanthanide NMR Probe 5 (CLaNP-5) readily attachable to a protein surface via two cysteine residues. The probe causes tunable pseudocontact shifts, alignment, paramagnetic relaxation enhancement, and luminescence, by chelating it to the appropriate lanthanide ion. The observation of single shifts and the finding that the magnetic susceptibility tensors obtained from shifts and alignment analyses are highly similar strongly indicate that the probe is rigid with respect to the protein backbone. By placing the probe at various positions on a model protein it is demonstrated that the size and orientation of the magnetic susceptibility tensor of the probe are independent of the local protein environment. Consequently, the effects of the probe are readily predictable using a protein structure only. These findings designate CLaNP-5 as a protein probe to deliver unambiguous high quality structural restraints in studies on protein−protein and protein−ligand interactions.

Introduction

Paramagnetic restraints obtained from NMR experiments have proven to be a powerful tool in the refinement of macromolecular structures and in gaining structural information on (transient) protein−protein and protein−ligand interactions.[1−4] Besides stabile radicals such as nitroxides,[5−7] lanthanide ions are generally applied as the source of the paramagnetic effects because the 4f-block family contains both diamagnetic and paramagnetic ions, the latter in varying strength and degree of anisotropy, which allows for a broad range of NMR experiments.[8,9] Ln ions can be readily interchanged, as their chemical and physical properties are highly similar. One approach to incorporate Ln ions into proteins is via the exchange for ionic cofactors such as Ca^{2+} and Mg^{2+}, yielding paramagnetic distance and angular restraints.[10−13] As a more widely applicable alternative, Ln ions can be specifically positioned onto any protein via Ln binding proteins and peptides,[14−16] or via modification of proteins with small synthetic Ln ligands.[17−21]

Two aspects of such synthetic probes are of particular importance. First, isomerization of the probe should be minimized. Ln ions favor coordination by eight or nine ligands and many Ln complexes exist in several isomers. Often these complexes have different magnetic susceptibilities, resulting in multiple NMR signals for every nucleus in the protein.[18,22] Thus, the Ln complex should be designed in such a way that isomerization is minimal and single signals are observed.

(1) Allegrozzi, M.; Bertini, I.; Janik, M. B.; Lee, Y. M.; Liu, G.; Luchinat, C. *J. Am. Chem. Soc.* **2000**, *122*, 4154–4161.
(2) Pintacuda, G.; Park, A. Y.; Keniry, M. A.; Dixon, N. E.; Otting, G. *J. Am. Chem. Soc.* **2006**, *128*, 3696–3702.
(3) Clore, G. M.; Tang, C.; Iwahara, J. *Curr. Opin. Struct. Biol.* **2007**, *17*, 603–616.
(4) Volkov, A. N.; Worrall, J. A.; Holtzmann, E.; Ubbink, M. *Proc. Natl. Acad. Sci. U.S.A.* **2006**, *103*, 18945–18950.
(5) Kale, S.; Ulas, G.; Song, J.; Brudvig, G. W.; Furey, W.; Jordan, F. *Proc. Natl. Acad. Sci. U.S.A.* **2008**, *105*, 1158–1163.
(6) Battiste, J. L.; Wagner, G. *Biochemistry* **2000**, *39*, 5355–5365.
(7) Lindfors, H. E.; de Koning, P. E.; Drijfhout, J. W.; Venezia, B.; Ubbink, M. *J. Biomol. NMR* **2008**, *41*, 157–167.
(8) Horrocks, W. D., Jr.; Sipe, J. P. *Science* **1972**, *177*, 994–996.
(9) Hinckley, C. C. *J. Am. Chem. Soc.* **1969**, *91*, 5160–5162.
(10) Biekofsky, R. R.; Muskett, F. W.; Schmidt, J. M.; Martin, S. R.; Browne, J. P.; Bayley, P. M.; Feeney, J. *FEBS Lett.* **1999**, *460*, 519–526.
(11) Barden, J. A.; Cooke, R.; Wright, P. E.; dos Remedios, C. G. *Biochemistry* **1980**, *19*, 5912–5916.
(12) Bertini, I.; Janik, M. B.; Lee, Y. M.; Luchinat, C.; Rosato, A. *J. Am. Chem. Soc.* **2001**, *123*, 4181–4188.
(13) Gay, G. L.; Lindhout, D. A.; Sykes, B. D. *Protein Sci.* **2004**, *13*, 640–651.
(14) John, M.; Pintacuda, G.; Park, A. Y.; Dixon, N. E.; Otting, G. *J. Am. Chem. Soc.* **2006**, *128*, 12910–12916.
(15) Su, X. C.; McAndrew, K.; Huber, T.; Otting, G. *J. Am. Chem. Soc.* **2008**, *130*, 1681–1687.
(16) Martin, L. J.; Hahnke, M. J.; Nitz, M.; Wohnert, J.; Silvaggi, N. R.; Allen, K. N.; Schwalbe, H.; Imperiali, B. *J. Am. Chem. Soc.* **2007**, *129*, 7106–7113.
(17) Leonov, A.; Voigt, B.; Rodriguez-Castaneda, F.; Sakhaii, P.; Griesinger, C. *Chem.—Eur. J.* **2005**, *11*, 3342–3348.
(18) Prudencio, M.; Rohovec, J.; Peters, J. A.; Tocheva, E.; Boulanger, M. J.; Murphy, M. E.; Hupkes, H. J.; Kosters, W.; Impagliazzo, A.; Ubbink, M. *Chem.—Eur. J.* **2004**, *10*, 3252–3260.
(19) Vlasie, M. D.; Comuzzi, C.; van den Nieuwendijk, A. M.; Prudencio, M.; Overhand, M.; Ubbink, M. *Chem.—Eur. J.* **2007**, *13*, 1715–1723.
(20) Rodriguez-Castaneda, F.; Haberz, P.; Leonov, A.; Griesinger, C. *Magn. Reson. Chem.* **2006**, *44 Spec No*, S10–16.
(21) Gaponenko, V.; Sarma, S. P.; Altieri, A. S.; Horita, D. A.; Li, J.; Byrd, R. A. *J. Biomol. NMR* **2004**, *28*, 205–212.

 10.1021/ja8054832 CCC: $40.75

Second, the position of the probe relative to the protein should be well defined.[15,23,24] Ln ions attached via flexible linkers show mobility causing averaging of the paramagnetic effects. In the case where the probe is used to obtain paramagnetic induced alignment in the magnetic field, mobility reduces the size of the observed residual dipolar couplings (RDCs).[22,25−27] The averaging is even more detrimental when distance information is to be gathered from pseudocontact shifts (PCSs) or paramagnetic relaxation enhancement (PRE) because both phenomena are strongly distance dependent. So in particular for application in structure determination of protein−protein and protein−ligand complexes, the location of the Ln ion relative to the protein needs to be well defined. For structure determination of large complexes in which the probe is attached to the larger macromolecule,[3,28] it is essential that the Ln ion position and also the direction and strength of the magnetic susceptibility tensor can be predicted solely on the basis of a structural model, because it is usually impossible to determine these experimentally.

Recently, we investigated the effects of the Caged Lanthanide NMR Probe 5 (CLaNP-5) when attached to a protein via one or two sulfide bridges.[29] Due to the presence of two pyridine-*N*-oxide ligating pendant arms CLaNP-5 is a C-2 symmetric, rigid probe relative to the protein backbone, giving single shifts and significant alignment and is, therefore, an improvement over the synthetic paramagnetic probes reported so far.[19] In this study the rigidity, the predictability of its paramagnetic parameters, and the general applicability of CLaNP-5 are examined. By using a set of lanthanides, several double cysteine mutants of the model protein pseudoazurin (Paz) and various NMR experimental techniques we show that the paramagnetic effect of CLaNP-5 is tuned by the chelated Ln ion and both strength and direction of this effect are independent of the protein environment. It is shown that ClaNP-5 is a widely applicable probe, ideally suited for paramagnetic structure refinement of macromolecules and their complexes.

Results

Synthesis of CLaNP-5 and its Protein Complexes. The challenges in the design of synthetic Ln-chelating protein probes comprise the needs for high affinity for Ln ions, minimal ligand isomerization, easy and site-specific attachment to proteins, and conformational restriction of the Ln caged complex relative to the protein.[17−19,22,30−32] The Ln complexing compound 1,4,7,10-tetraazacyclododecane-1-[N-oxido-pyridine-2-ylmethyl]-4,7,10-triacetic acid (H_3DO3A-pyNox) is a highly rigid Ln chelator, reported to adopt a single isomer conformation.[33] These favorable properties were applied in the design and construction of the protein probe. For symmetry reasons CLaNP-5 was designed to have a 2-fold rotational axis, bearing two activated thiol spacers on opposite pendant arms, attachable to two cysteine residues and two opposite pyridine-N-oxide pendant arms to minimize ring and side chain isomerization.[33] CLaNP-5 was synthesized according to Scheme 1. Thus, commercially available 2-(hydroxymethyl)-pyridine (**1**) was oxidized using MCPBA and subsequently transformed into the chloride **3** in 92% yield over two steps. Chloride **3** was used to bialkylate the cyclen derivative **4** to give the diacid **5** after deprotection using TFA. Condensation of **5** with excess 2-(aminoethyl)-methanethiosulfonate in presence of EDC and NHS provided CLaNP-5 (**6**) in 84% yield. After considerable experimentation, quantitative yields of Ln-CLaNP-5 (**7a**−**f**) were obtained when the ligation reaction of Ln ions to **6** was performed in DMF using Ln acetate salts. (When the reaction was performed in water using Ln nitrate salts, the ligation was less efficient, breakdown products of CLaNP-5 were detected in LCMS analyses of crude reactions and additional HPLC purification was necessary before the attachment of Ln-ClaNP-5 to the protein.)

CLaNP-5, chelated to the appropriate Ln ion, was attached to double cysteine mutants of the blue copper protein pseudoazurin (Paz) to give the modified protein complexes (**8a**−**j**). The cysteine positions were designed on the protein surface, with their Cα atoms between 6−10 Å apart, their sidechains pointing away from the protein and in the same direction.

Magnetic Susceptibility Tensor Determination Using PCS. For the application of CLaNP-5 as a paramagnetic probe in structure determination of proteins and their complexes, knowledge of its magnetic susceptibility tensor (χ-tensor) is required. The χ-tensor can be characterized by measuring PCSs caused by Ln-CLaNP-5 on nuclei of a small protein for which the structure is available. It was previously shown that attachment of Yb-CLaNP-5 to Paz with mutations E51C/E54C (**8b**) gave single PCSs, and using the crystal structure of a similar type of probe (CLaNP-1) attached to the same protein (PDB entry 1PY0), the χ-tensor could be estimated.[29] For accurate χ-tensor determination, it is crucial to obtain the Ln ion position in CLaNP-5 relative to the attached protein. In this study, the Ln ion position was modeled by using restraints based on PCSs from Yb-CLaNP-5 attached to Paz E51C/E54C. As additional restraints, Yb was restricted 8 ± 2 Å away from the cysteine Cα atoms. These distances are based on the Ln ion to cysteine Cα distances in 1PY0 and on a model of CLaNP-5 attached to cysteine residues created with Spartan ʼ04 (www.wavefun.com), which yielded distances of 7.9 and 8.3 Å. Based on the structural model of the probe, the Lennard-Jones potential parameters of the Ln ion were adjusted to an ionic radius of 6 Å, matching the distance of the Ln ion to the pyridine protons. With the obtained Yb position, the sizes of the axial and rhombic components of the χ-tensor ($\Delta\chi_{ax}$ and $\Delta\chi_{rh}$) could be estimated, and these values were used to predict the Ln ion position more accurately. This iterative procedure led to convergence and the ultimate position of Yb is shown in Figure 1A.

Ln Ion Position Validation Using PRE. To independently determine the position of the Ln ion relative to the protein

(22) Ikegami, T.; Verdier, L.; Sakhaii, P.; Grimme, S.; Pescatore, B.; Saxena, K.; Fiebig, K. M.; Griesinger, C. *J. Biomol. NMR* **2004**, *29*, 339–349.
(23) Bertini, I.; Gupta, Y. K.; Luchinat, C.; Parigi, G.; Peana, M.; Sgheri, L.; Yuan, J. *J. Am. Chem. Soc.* **2007**, *129*, 12786–12794.
(24) Su, X. C.; Man, B.; Beeren, S.; Liang, H.; Simonsen, S.; Schmitz, C.; Huber, T.; Messerle, B. A.; Otting, G. *J. Am. Chem. Soc.* **2008**, *130*, 10486–10487.
(25) Gaponenko, V.; Dvoretsky, A.; Walsby, C.; Hoffman, B. M.; Rosevear, P. R. *Biochemistry* **2000**, *39*, 15217–15224.
(26) Zhuang, T.; Lee, H. S.; Imperiali, B.; Prestegard, J. H. *Protein Sci.* **2008**,
(27) Wohnert, J.; Franz, K. J.; Nitz, M.; Imperiali, B.; Schwalbe, H. *J. Am. Chem. Soc.* **2003**, *125*, 13338–13339.
(28) Vlasie, M. D.; Fernandez-Busnadiego, R.; Prudencio, M.; Ubbink, M. *J. Mol. Biol.* **2008**, *375*, 1405–1415.
(29) Keizers, P. H.; Desreux, J. F.; Overhand, M.; Ubbink, M. *J. Am. Chem. Soc.* **2007**, *129*, 9292–9293.
(30) Spirlet, M. R.; Rebizant, J.; Desreux, J. F.; Loncin, M. F. *Inorg. Chem.* **1984**, *23*, 359–363.
(31) Desreux, J. F. *Inorg. Chem.* **1980**, *19*, 1319–1324.
(32) Di Bari, L.; Pescitelli, G.; Sherry, A. D.; Woods, M. *Inorg. Chem.* **2005**, *44*, 8391–8398.
(33) Polasek, M.; Rudovsky, J.; Hermann, P.; Lukes, I.; Elst, L. V.; Muller, R. N. *Chem. Commun. (Cambridge, U. K.)* **2004**, 2602–2603.

Scheme 1. Synthesis and Protein Attachment of CLaNP-5[a]

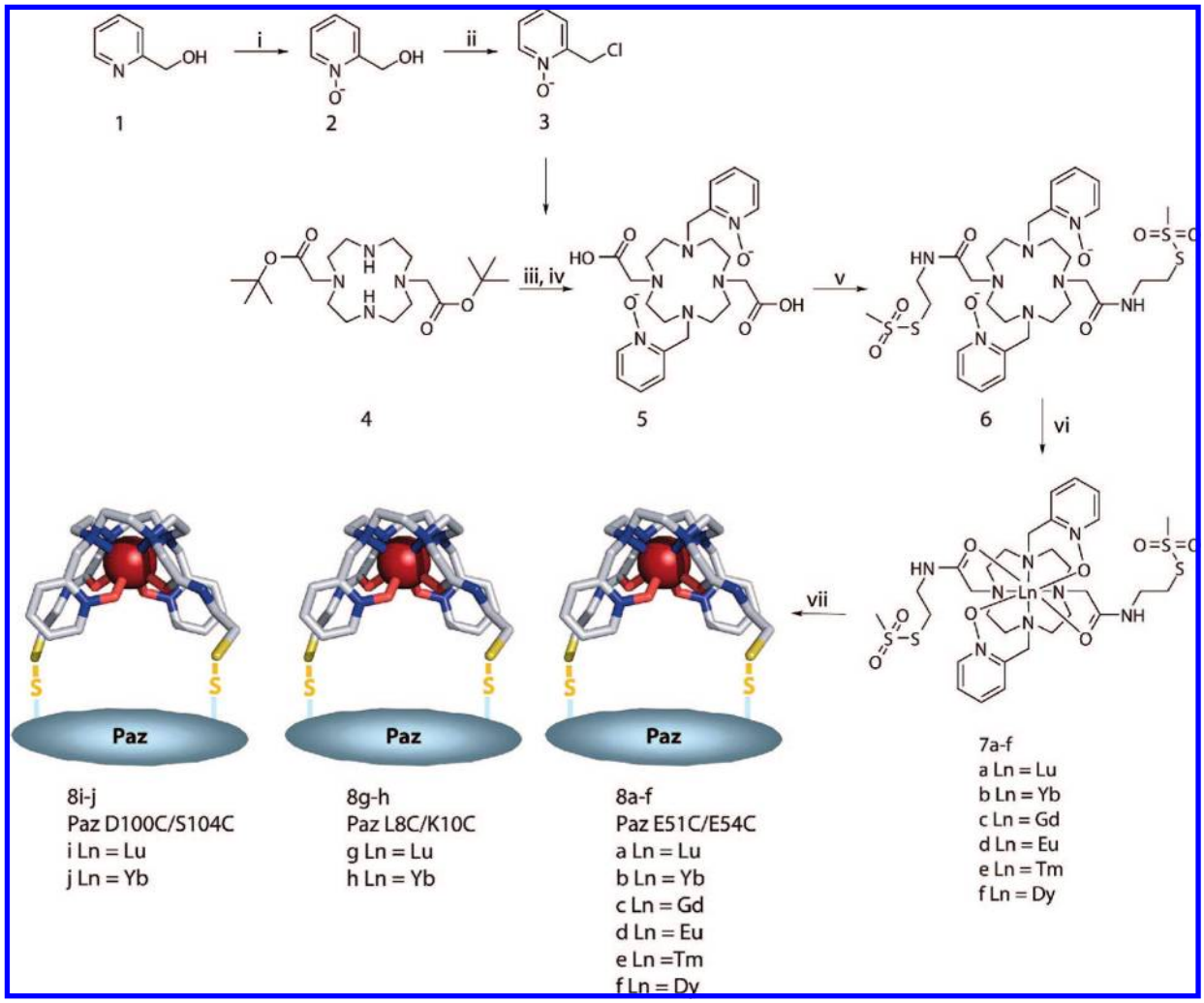

[a] Reagents and conditions: (i) *m*CPBA, $CHCl_3$, 16 h, RT, 98%; (ii) $SOCl_2$, CH_2Cl_2, reflux, 2 h, 94%; (iii) $ClCH_2$pyNox (**3**), MeCN, K_2CO_3, 24 h, 80 °C; (iv) TFA, CH_2Cl_2, 4 h, RT; (v) aminoethyl-MTS, NHS, EDC, DMF, 30 h, RT, HPLC, iii−v 84%; (vi) $Ln(OAc)_3$, DMF, 1 h, RT, quant; (vii) DTT prereduced Paz double Cys mutant, 20 mM sodium phosphate, pH 7.0, 150 mM NaCl, 1 h, 4 °C, FPLC, 50−90%. The structural model of **7** was created using Spartan '04.

backbone in CLaNP-5 attached to Paz, Gd-CLaNP-5 was attached to Paz E51C/E54C (**8c**). The Gd ion causes PREs of the protein resonances containing Ln ion to nucleus distance information. The PRE-based optimal Ln ion position was found in between C51 and C54 at distances of 7.4 and 9.1 Å from the Cα atoms, respectively (Figure 1A). This position matches the expectations based on the structural model of CLaNP-5 and resembles the positions of Gd in CLaNP-1 and CLaNP-3 attached to Paz E51C/E54C.[19] The experimentally determined (Supporting Information Figure S1) and back-calculated distances between the amide protons and the Gd ion all correlate within a 3 Å range (Figure 1B). Resonances of nuclei that are broadened beyond detection are given an upper limit of 20 Å from the Gd ion. Similarly, nuclei of which the resonances are unaffected are given a lower limit of 31 Å.

The position of the Gd ion was located at 2.0 Å from the position of the Yb ion, determined via PCS analysis. To determine whether the difference in these positions can be explained by the experimental error, the PRE-based Ln ion position calculations were repeated 25 times with 20% noise randomly added to the R_2^{para} values. The noise is estimated based on the standard deviation in background signal of the [^{15}N, ^{1}H]-HSQC spectra, which is around 5% of the average peak signal. This noise will cause errors in determining both the intensity ratios and the linewidths of the resonances, estimated to affect the PREs maximally to 20%. The cloud of the 25 positions overlaps with the Ln ion position determined via PCSs (Figure 1B).

Magnetic Susceptibility Tensors of Various Ln Ions in CLaNP-5. The maximum distance from the probe at which significant PCSs of the protein nuclei resonances are observed depends primarily on the intrinsic strength of the ligated Ln ion. Yb exerts effects over 35 Å, affecting almost all nuclei of Paz, but for large complexes of proteins even more distant effects are desirable. Therefore, a set of Ln ions was chelated to CLaNP-5 and attached to Paz E51C/E54C (**8a**−**f**). Besides Yb, Eu was selected as a weak anisotropic paramagnetic Ln ion that also has fluorescent properties. Dy and Tm were used because these represent two of the strongest anisotropic paramagnetic Ln ions.[12] Lu-ligated CLaNP-5 attached to Paz E51C/E54C served as a diamagnetic control. Significant shifts in the [^{15}N, ^{1}H]-HSQC spectra were observed for all anisotropic paramagnetic Ln ions, the PCSs caused by Tm (**8e**) are exemplified in Figure 2A. Eu caused the smallest and Tm the

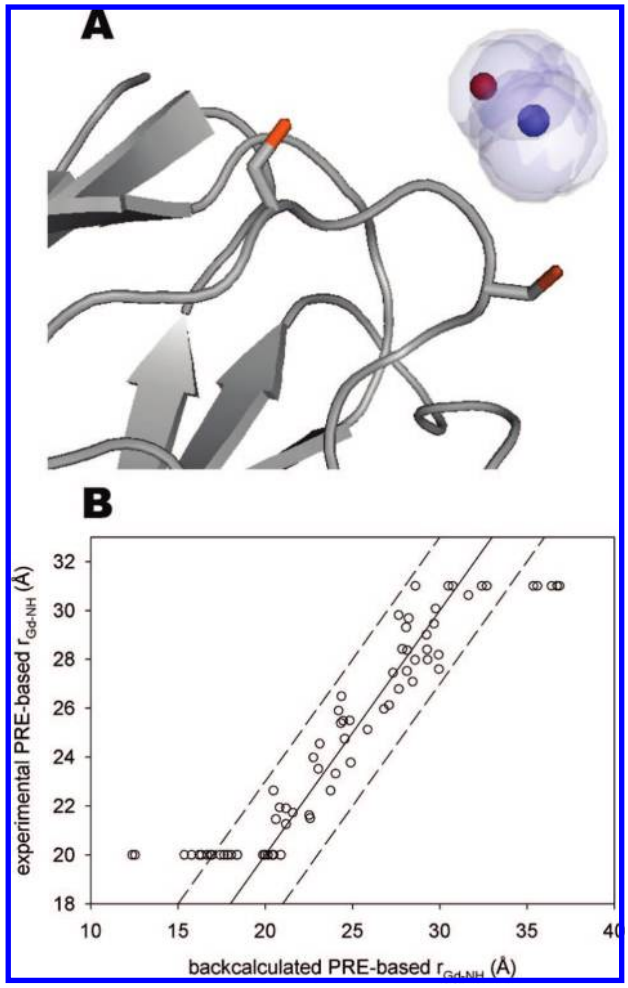

Figure 1. Optimized positions of Ln ions relative to the Paz E51C/E54C structure (A). The red sphere represents the PCS-based position of Yb, the blue sphere represents the PRE-based position of Gd and the transparent cloud represents PRE-based Gd surfaces obtained including 20% artificial noise. Residues 51 and 54 are depicted as sticks, the picture was made using Pymol v0.99 (www.pymol.org). The experimentally observed Gd to amide proton distances (Å) are plotted against the back-calculated distances (B). A solid line indicates the ideal correlation; dashed lines represent ±3 Å limits ($Q = 0.10$).

largest shifts, whereas Dy only gave negative shifts. PCSs were measured for all Ln ions and the χ-tensor parameters were determined by using the PCS-based Ln ion position determined for Yb-CLaNP-5 (Table 1). The observed PCSs and the fit of experimental versus back-calculated PCSs using Tm are shown in Figure 2, those of the other Ln ions in the Supporting Information (Figure S2). The χ-tensor is smallest for Eu and largest for Tm. Dy yielded a negative χ-tensor that is smaller in size than that of Tm. Only the γ-Euler rotation angle was found to differ significantly between the Ln ions. This angle is underdetermined for Eu, probably due to a negligible rhombicity of its χ-tensor. Also, in general, the γ Euler angle is often underdetermined, as has been reported before by others.[34,35] The α and β Euler angles are similar for all Ln ions, indicating the χ-tensor direction to be dictated by the probe, rather than the ligated metal.

Alignment by CLaNP-5. To establish the degree of alignment caused by Ln-CLaNP-5 attached to Paz E51C/E54C, RDCs were determined for the amides with well-separated and reliably assigned resonances. From the RDCs the χ-tensors were calculated. Fitting of the RDCs to the crystal structure of Paz with its amide proton positions predicted in X-PLOR-NIH did not give satisfactorily results. Furthermore, the RDC-based χ-tensor sizes were on average 35% smaller than those obtained from the PCS analysis. Therefore, the Paz protein structure was first optimized using all experimental RDC data as restraints before using it to calculate the individual χ-tensor parameters for each Ln ion. The subsequently obtained RDC-based χ-tensor parameters match well with the ones obtained via PCS analysis (Table 2). Intrinsic protein mobility can be another cause of deviation of the observed versus the calculated RDCs and, thus, ensemble-averaging approaches would be required for further optimization of the analysis.[36−38] Such approaches are not included in this study, as the goal is not to optimize the Paz structure but to validate the Ln-CLaNP-5 χ-tensors.

To validate the PCS-based χ-tensors, the experimentally obtained RDCs were plotted versus predicted RDCs, calculated using the PCS-based χ-tensors. The fit of the effect of Tm is shown as an example in Figure 2E, those of the other Ln ions are shown in the Supporting Information, Figure S3. The predicted versus observed RDCs gave a reasonable fit for Yb and good fits for Tm and Dy. The fit for Eu was poor because of the small χ-tensor and the subsequent small degree of alignment. The RDCs of Yb-CLaNP-5 attached Paz were also determined at 21.1 T, yielding values ranging from −8 to 9 Hz (data not shown), 2-fold larger than at 14.1 T. This is in line with the B_0^2 dependence of the size of RDCs. For protein structure refinement by RDC restraints using CLaNP-5 at 14.1 T, strong Ln ions like Tm or Dy should be used.

Fluorescence of Eu-CLaNP-5. The absorbance spectrum of CLaNP-5 changes upon ligation to Eu. The absorbance maximum increases and changes from 260 nm to 250 and 210 nm. Upon excitation at 250 nm Eu-CLaNP-5 (**7d**) emits at 590, 617 and 700 nm in sharp bands typical for Ln-based fluorescence (Figure 3A). The lifetime of the luminescence at 617 nm is estimated 0.503 ± 0.002 ms based on exponential curve fitting (Figure 3B). These fluorescent properties of Eu-CLaNP-5 are useful to detect probe-attached protein.

Effects of Yb-CLaNP-5 Attached to Paz at Different Positions. A promising application of paramagnetic probes is in the study of protein complexes. In such cases, the probe is attached to a NMR silent (i.e., not isotope enriched) binding partner and its effect on the other protein is observed.[3,4,28] In those cases, a priori knowledge of the strength and direction of the paramagnetic probe is required for the use of PCSs or RDCs, and these parameters should be independent of the protein. To test this, Lu- and Yb-CLaNP-5 were placed on two more positions on the surface of Paz, using the mutants L8C/K10C and D100C/S104C (**8g**−**j**). Yb was selected for these experiments because it was found to give significant alignment and shifts for most residues without large broadening. In a procedure analogous to the one described above for the E51C/E54C

(34) Schmitz, C.; John, M.; Park, A. Y.; Dixon, N. E.; Otting, G.; Pintacuda, G.; Huber, T. *J. Biomol. NMR* **2006**, *35*, 79–87.
(35) Su, X. C.; Huber, T.; Dixon, N. E.; Otting, G. *ChemBioChem* **2006**, *7*, 1599–1604.
(36) Clore, G. M.; Schwieters, C. D. *J. Am. Chem. Soc.* **2004**, *126*, 2923–2938.
(37) Lindorff-Larsen, K.; Best, R. B.; Depristo, M. A.; Dobson, C. M.; Vendruscolo, M. *Nature* **2005**, *433*, 128–132.
(38) Lange, O. F.; Lakomek, N. A.; Fares, C.; Schroder, G. F.; Walter, K. F.; Becker, S.; Meiler, J.; Grubmuller, H.; Griesinger, C.; de Groot, B. L. *Science* **2008**, *320*, 1471–1475.

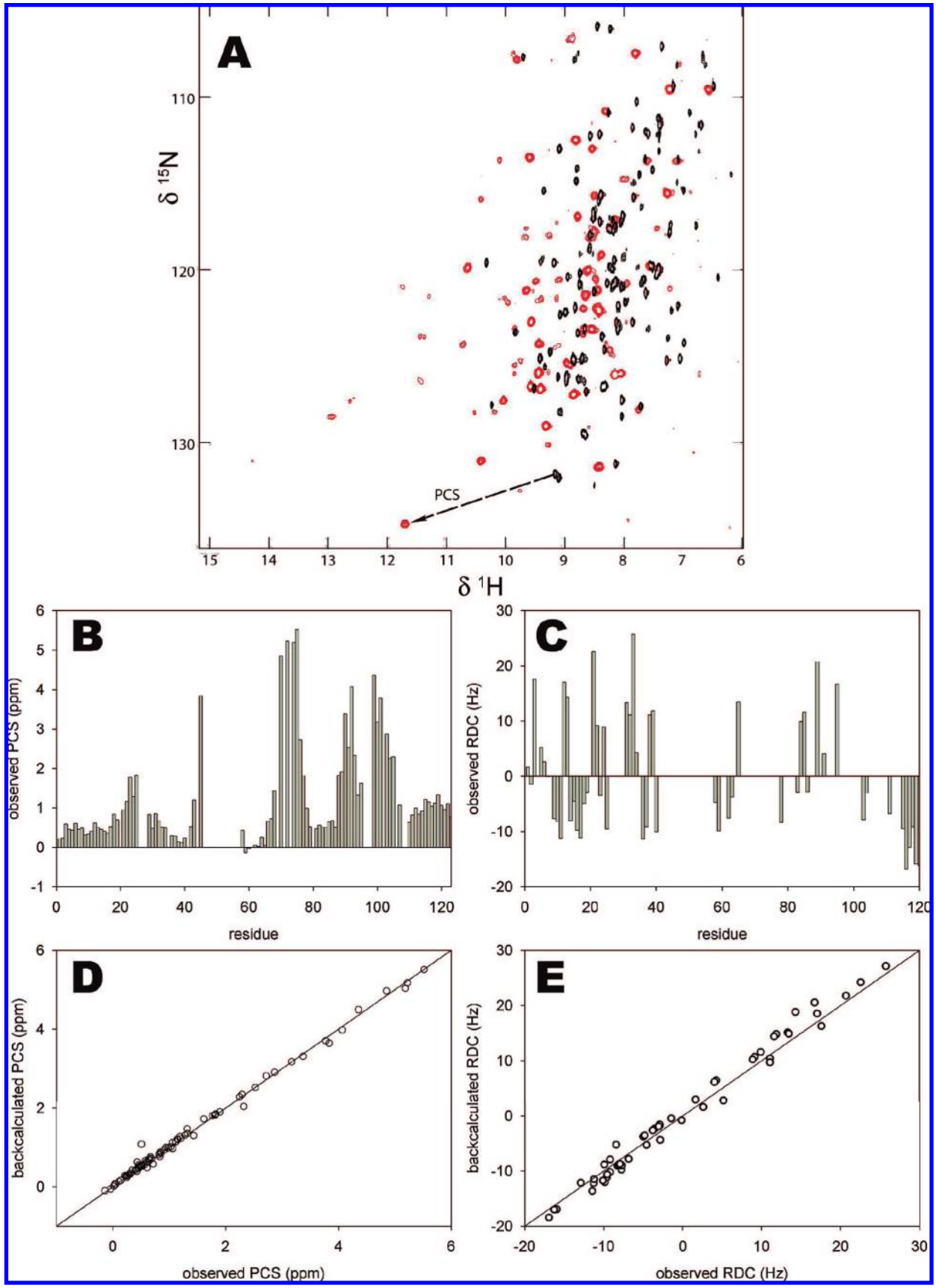

Figure 2. Overlay of [^{15}N, ^{1}H]-HSQC spectra of Paz E51C/E54C attached to Lu-CLaNP-5 (black) and Tm-ClaNP-5 (red) (A). Experimentally observed PCSs (ppm) and RDCs (Hz) of Tm-CLaNP-5 attached to Paz E51C/E54C are displayed per residue (B and C, respectively) and plotted against the backcalculated PCSs and RDCs (D and E, respectively) using the χ-tensor parameters in Table 1. The ideal correlations are shown as solid lines.

Table 1. PCS-Based χ-Tensor Parameters of Ln-CLaNP-5 attached to Paz E51C/E54C[a]

Ln	Yb	Eu	Tm	Dy
$\Delta\chi_{ax}$	9.0 ± 0.1[b]	1.49 ± 0.03	55.3 ± 0.3	−36.2 ± 0.7
$\Delta\chi_{rh}$	2.3 ± 0.3[b]	0.1 ± 0.2	6.9 ± 2	−15.0 ± 2
α	109.5 ± 0.4	103 ± 1	114.1 ± 0.4	101 ± 1
β	84.3 ± 0.5	82 ± 1	81.0 ± 0.3	88.4 ± 0.6
γ	−53 ± 8	47 ± 56	−51 ± 6	−85 ± 6
restraints	94	94	89	75
range[c]	0.05/1.95	−0.02/0.37	−0.14/5.5	−2.8/0.01
Q	0.10	0.21	0.11	0.18

[a] The axial and rhombic components ($\Delta\chi_{ax}$ and $\Delta\chi_{rh}$ in 10^{-32} m^3) and the Euler rotation angles (α, β, and γ, in degrees) to rotate the protein into the χ-tensor frame were calculated using the observed PCSs and protein structure 1PY0. [b] The previously reported values[29] are in the wrong units. [c] The largest observed PCSs (ppm) are indicated.

Table 2. RDC-Based χ-Tensor Parameters of Ln-CLaNP-5 attached to Paz E51C/E54C[a]

Ln	Yb	Eu	Tm	Dy
$\Delta\chi_{ax}$	8.4 ± 0.5[b]	−1.4 ± 0.4	44.4 ± 0.5	−34.6 ± 0.7
$\Delta\chi_{rh}$	2.0 ± 0.7[b]	−0.7 ± 0.3	6.9 ± 0.5	−11.0 ± 0.7
restraints	48	87	53	32
range[c]	−4/6	−3/3	−20/26	−20/18
Q	0.46	0.96	0.15	0.23

[a] The axial and rhombic components ($\Delta\chi_{ax}$ and $\Delta\chi_{rh}$ in 10^{-32} m^3) were calculated using the observed RDCs and the optimized 1PY0-based protein structure. [b] The previously reported values[29] are in the wrong units. [c] The largest observed RDCs (Hz) are indicated.

mutant, these two probe-attached mutants were subjected to PCS and RDC analysis to determine and validate the χ-tensors. The experimental values and the fits of experimental versus calculated PCSs and RDCs are shown in the Supporting Information, Figures S4 and S5, respectively. The calculated χ-tensor parameters are summarized in Tables 3 and 4 for PCSs and RDCs, respectively. In general, the RDC-based χ-tensors are lower than the PCS-based ones. However, when the PCS-based χ-tensors are used to back-calculate RDCs, fits of similar quality are obtained (Q-values 0.51, 0.46, and 0.60 for PCS-based χ-tensors and 0.53, 0.47, and 0.48 for RDC-based χ-tensors, respectively). This indicates that the PCS-based χ-tensors explain the observed RDCs equally well. The Q-values are higher for RDC than for PCS data because the error in the RDCs is larger and the RDCs are much more sensitive to differences in structure and dynamics between crystal and solution structures.

Apparently, the position of the Ln ion can be predicted accurately as the observed PCSs fit well to the backcalculated. It can be concluded that the protein environment does not influence the size of the paramagnetic effect of the probe. The directions of the χ-tensors are displayed in Figure 4. In all three cases the axial component of the χ-tensor is pointing away from the protein surface and the *x*-component is on average making a 20° angle (ranging from −2° to 45°) with the Cα-Cα vector connecting the two cysteine residues. To compare the directions of the χ-tensors on the different mutants, these are aligned in Figure 4D. The directions of the principal axes of the χ-tensor relative to the cysteine Cα atoms are similar for the three mutants, indicating that these are mainly determined by the CLaNP-5 ligand.

Predicting PCS. The observed independence of the χ-tensor parameters on the protein environment suggests that it is possible to predict the Ln position and the χ-tensor with reasonable accuracy for a given protein structure. First, two surface residues to be mutated to the cysteines attaching CLaNP-5 are selected.

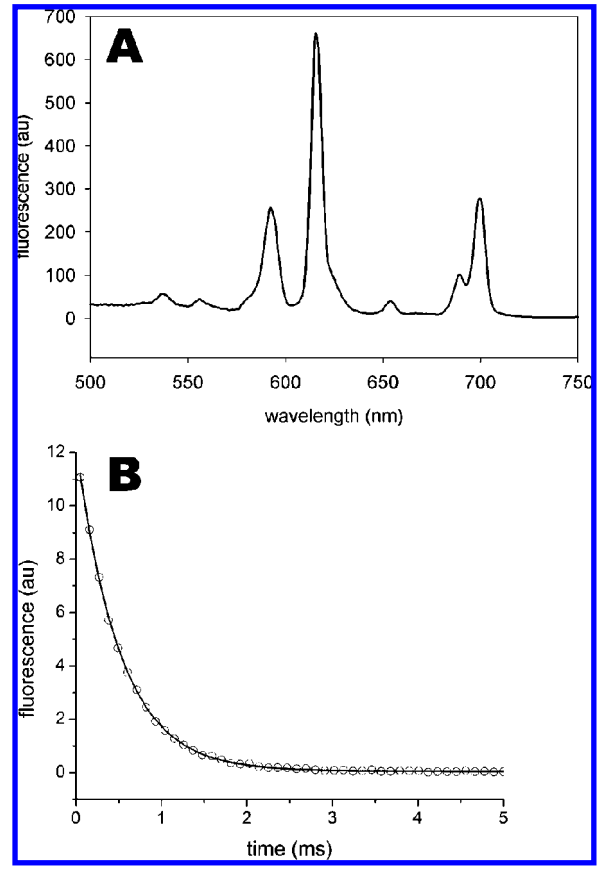

Figure 3. Emission spectra of 100 μM Eu-CLaNP-5, using an excitation wavelength of 250 nm (A) and fluorescence decay of Eu-CLaNP-5 (B). The measured points (○) and the exponential fit (solid line) are indicated.

Table 3. PCS-Based χ-Tensor Parameters of Yb-CLaNP-5 attached to Paz L8C/K10C, E51C/E54C, and D100C/S104C[a]

mutant	L8C/K10C	E51C/E54C	D100C/S104C
$\Delta\chi_{ax}$	9.0 ± 0.1	9.0 ± 0.1	9.3 ± 0.2
$\Delta\chi_{rh}$	3.3 ± 0.2	2.3 ± 0.3	3.0 ± 0.4
restraints	81	94	96
Q	0.10	0.10	0.11

[a] The axial and rhombic components ($\Delta\chi_{ax}$ and $\Delta\chi_{rh}$ in 10^{-32} m^3) were calculated using the observed PCSs and protein structure 1PY0.

Table 4. RDC-Based χ-Tensor Parameters of Yb-CLaNP-5 attached to Paz L8C/K10C, E51C/E54C, and D100C/S104C[a]

mutant	L8C/K10C	E51C/E54C	D100C/S104C
$\Delta\chi_{ax}$	7.5 ± 0.5	8.4 ± 0.5	5.8 ± 0.5
$\Delta\chi_{rh}$	2.3 ± 0.6	2.0 ± 0.7	1.7 ± 0.5
restraints	67	48	80
Q	0.53	0.47	0.48

[a] The axial and rhombic components ($\Delta\chi_{ax}$ and $\Delta\chi_{rh}$ in 10^{-32} m^3) were calculated using the observed RDCs and the optimized 1PY0-based protein structure.

These residues should be roughly 8 Å apart with their sidechains pointing away from the surface. If a protein complex is investigated, the mutations should be placed far enough from a putative binding site, yet close enough to yield appreciable paramagnetic effects; so roughly between 15−30 Å. Then the tensor frame is placed at 8 Å from the Cα of the residues to be mutated, with the *x*-axis making a 20° angle with the Cα-Cα vector of the two mutated residues and the *z*-axis pointing in the direction of the sidechains (see the Experimenal Section).

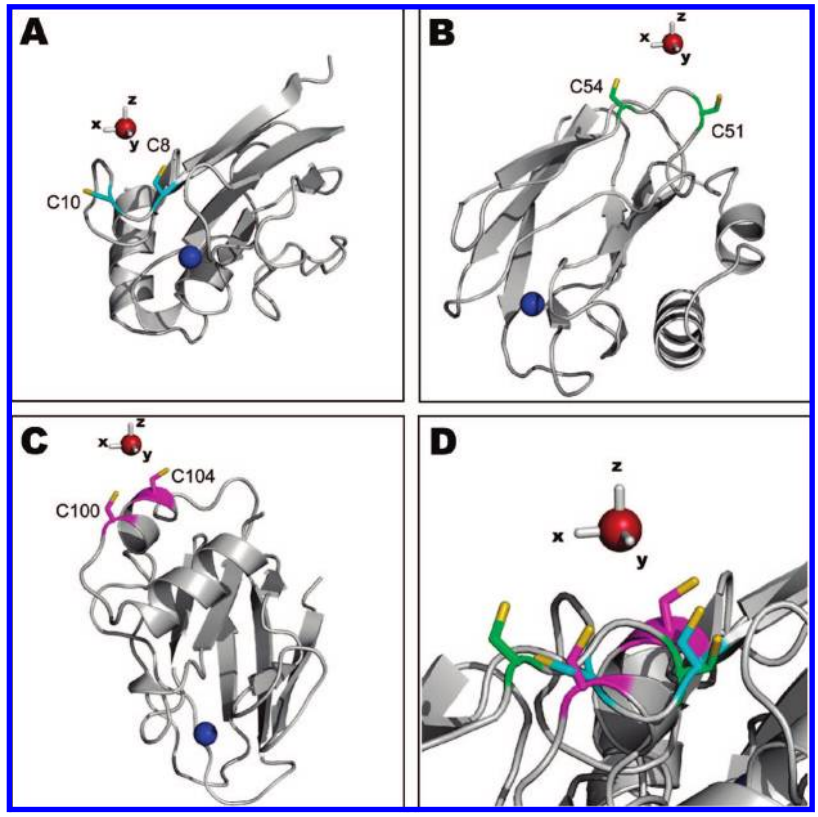

Figure 4. PCS-based positions of the principal axes of the χ-tensor of Yb-CLaNP-5 relative to the Paz structure (PDB entry 1PY0) for the mutants L8C/K10C (A), E51C/E54C (B), D100C/S104C (C), and all three aligned by the χ-tensor (D). Yb is displayed as a red sphere, the Cys sidechains as cyan (8C/10C), green (51C/54C), and magenta (100C/104C) sticks, and the Paz Cu atom as a blue sphere.

This simple procedure was applied to Paz for the three probe positions discussed above. Subsequently, the PCSs were calculated without applying any fitting to experimental data. The predicted PCS are plotted against the experimental data in Figure 5. As can be seen from the plots, the PCSs caused by CLaNP-5 can be predicted a priori sufficiently well to supply useful restraints, for example for docking of a protein−protein complex. To keep the procedure simple and general, outliers have not been studied in detail and optimization of the protocol is possible. For instance, in the docking of protein complexes the χ-tensor orientation may be iteratively optimized in parallel.

Discussion

Previously, we showed that Yb-CLaNP-5 is superior to many other synthesized Ln probes, by causing single PCSs of protein amide resonances and that protein attachment of the probe via two of its pendant arms instead of one increased the size of its paramagnetic effect significantly.[29] To apply CLaNP-5 as a paramagnetic probe to explore protein−ligand and protein−protein interactions, more stringent spectroscopic properties are required: When CLaNP-5 is to be used on macromolecules for which the χ-tensor cannot be determined, these properties need to be predicted. By using a set of six Ln ions and three Paz double cysteine mutants, it is shown that the position of the Ln ion relative to the protein is readily predictable, yielding satisfactory fits of backcalculated versus observed PCSs. Furthermore, the size and the direction of the χ-tensor of Yb-CLaNP-5 are highly similar for the three Paz mutants and therefore independent of protein surroundings. The paramagnetic strength of CLaNP-5 and, thereby, the range of distances yielding significant PCSs, is tunable by choosing the appropriate Ln ion. These properties make the paramagnetic effects of CLaNP-5 readily predictable to reasonable extent (Figure 5), using merely a structure of the protein to be probed.

The NMR spectra of a Lu-**5** complex indicate that the probe has some conformational freedom in solution when it is not bound to a protein (see the Experimental Section). This is indicated by the large linewidths of the polyaza proton peaks, which become more apparent at elevated temperatures, and this is strengthened by the positive sign of the crosspeaks between the polyaza CH_2 groups neighboring the acetate pendant arms in a NOESY spectrum, which are indicative of exchange. It is likely that the probe conformation is more restrained when attached to the protein. Whether the probe is conformationally fully restricted when immobilized is not clear. No doubling of resonances is observed in any of the protein [^{15}N, ^{1}H]-HSQC spectra, however, not even when using the strong paramagnet Tm for which shifts up to 6 ppm could still be assigned. Nevertheless, significant broadening was observed for the paramagnetically shifted resonances. This broadening occurs with all Ln ions but is most striking with Dy and Tm, where broadening of up to 50 Hz was observed. Paramagnetic relaxation, known to cause peak disappearance of nearby residues when using strong Ln ions,[27,39] can be ruled out as the origin of this broadening, because there is no relation between the linewidth and the distance to the Ln ion (Figure 6) or between the linewidth and the size of RDC or PCS. Conformational exchange of the probe is not likely to cause the broadening either, because not all resonances display an

(39) John, M.; Park, A. Y.; Dixon, N. E.; Otting, G. *J. Am. Chem. Soc.* **2007**, *129*, 462–463.

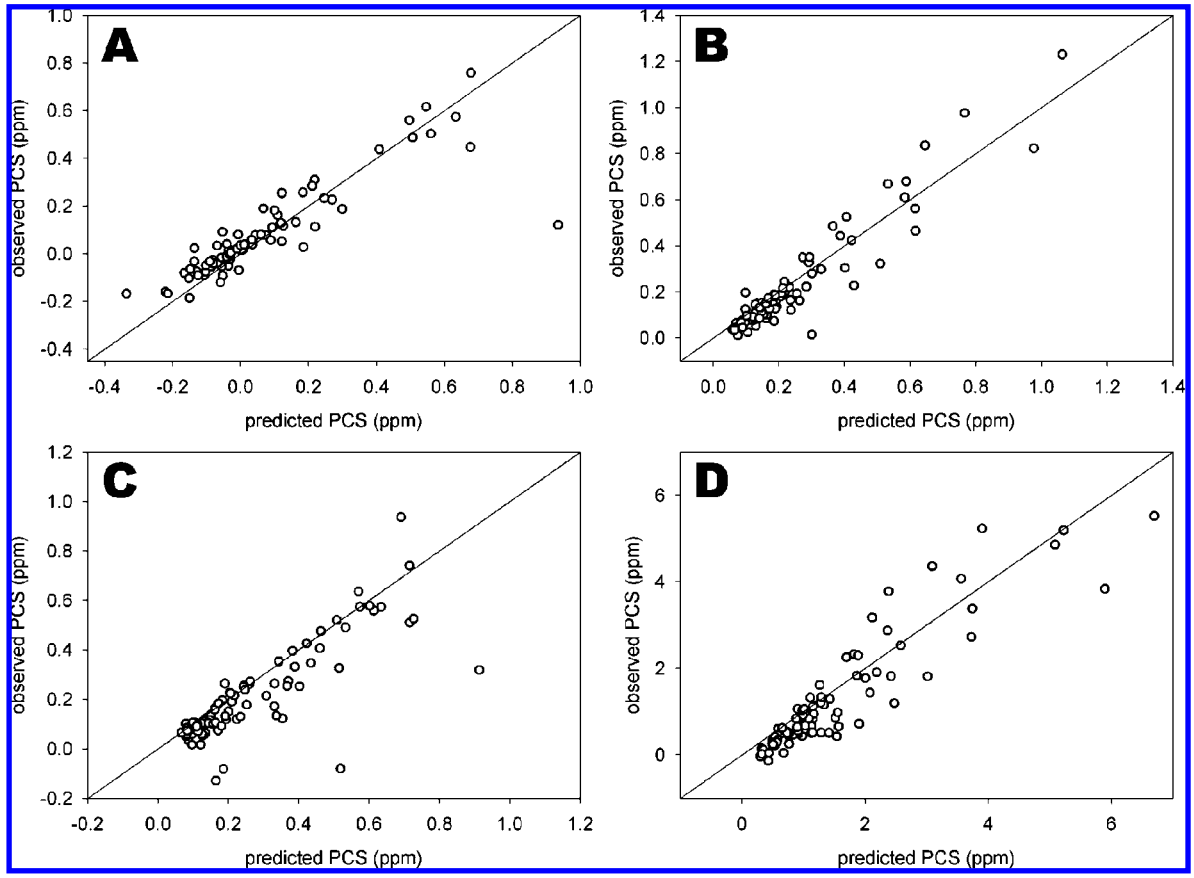

Figure 5. Predicted PCS (ppm) plotted against the experimentally obtained data of Yb-CLaNP-5 attached to Paz mutants L8C/K10C (**8j**, A, $Q = 0.55$), E51C/E54C (**8b**, B, $Q = 0.25$), and D100C/S104C (**8h**, C, $Q = 0.44$) and Tm-CLaNP-5 attached to Paz E51C/E54C (**8e**, D, $Q = 0.32$). The ideal correlations are indicated. The Ln ion position and the directions of the principal axes of the χ-tensor are predicted as described in the Experimental Section.

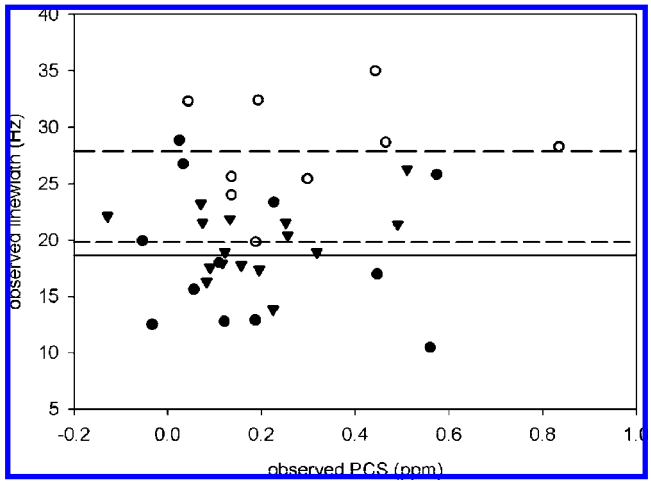

Figure 6. Linewidths (Hz) of a random set of HN-resonances of Yb-CLaNP-5 attached to Paz plotted against their PCSs (ppm). The individual signals and the averages of L8C/K10C (●, fine dashed line), E51C/E54C (○, course dashed line), and D100C/S104C (▼, solid line) are indicated. HN-resonances and PCSs were obtained from [^{15}N, ^{1}H]-HSQC spectra, the linewidths were determined from Lorentzian fitting using MestRec.

increased linewidth, and those that do are distributed all over the protein. Another explanation involves local flexibility of the protein. A loop-attached probe may move relative to the protein core even though being attached fully rigidly. In Paz, residues 100 and 104 are part of an α-helix and residues 8 and 10 are part of a β-sheet. Residues 51 and 54 are part of a loop and, therefore, a probe attached to these residues could be less restricted in its motions. To verify this explanation for the observed broadening, the linewidths of a random set of HN-resonances of the Yb-CLaNP-5 attached Paz samples were determined and plotted versus their PCSs (Figure 6). A wide distribution of linewidths is observed, but no trend is apparent between PCS and linewidth. Nevertheless, there are clear differences between the mutants. The linewidths for the E51C/E54C mutant are significantly increased, relative to the other two mutants of Paz, suggesting a relation between local protein flexibility and the observed line broadening.

The PCSs caused by Dy-CLaNP-5 were of less quality than those obtained using the other Ln ions. Furthermore, the negative value of the χ-tensor causes many signals to get lost in the water signal in the NMR spectrum. All together this resulted in the assignment of less peaks and a relatively poor correlation between backcalculated versus observed PCSs. Despite the limited quality of the data, it is clear that Dy-CLaNP-5 yields a smaller χ-tensor than Tm-CLaNP-5. This is also borne out by the smaller RDCs caused by Dy. Yet Dy has been reported to have a stronger paramagnetic effect than Tm.[12,40,41] The reason for this behavior remains unclear.

With PCSs up to 6 ppm and RDCs up to 26 Hz at 14.1 T, Tm-CLaNP-5 has a larger paramagnetic effect than Tm immobilized to peptide tags or interchanged for Ca^{2+} in EF-hand

(40) Barbieri, R.; Bertini, I.; Cavallaro, G.; Lee, Y. M.; Luchinat, C.; Rosato, A. *J. Am. Chem. Soc.* **2002**, *124*, 5581–5587.
(41) Mustafi, S. M.; Mukherjee, S.; Chary, K. V.; Cavallaro, G. *Proteins* **2006**, *65*, 656–669.

type proteins.[12,15,35] Again the rigidity of CLaNP-5 may play a role but also the number of ligands, which is 8 in CLaNP-5 and mostly up to 6 in Ln binding proteins or peptides, could be influencing the paramagnetic strength of the ion.

Several NMR techniques were successfully applied to retrieve protein structural restraints using CLaNP-5. Significant alignment is already caused by CLaNP-5 chelated to a weak paramagnetic Ln at 14.1 T, the field strength used in this study. Due to intrinsic alignment of the protein or because of rotational or conformational freedom of the alignment agent relative to the protein, the alignment tensor is usually smaller than the PCS-based tensor.[15] In this study the differences in size of the χ-tensors determined from alignment and shifts are small, as indicated by the similarities in the χ-tensor parameters determined via the two techniques (Tables 14) and the good fits of experimental versus predicted RDCs using the PCS-determined χ-tensor values. This strengthens the hypothesis that CLaNP-5 is rigidly attached to the protein compared to the protein backbone movements.

PRE was used in this study only to verify the Ln ion position with respect to the protein backbone, but it is a proven powerful tool to determine the structure of complexes of proteins.[28,42,43] The benefit of using PREs over PCSs is that no χ-tensor is involved in the calculations and the paramagnetic effects can be directly related to distances. The advantage of using PCSs is that potentially more long-range distance information is gained because PCSs decrease with the third power of the distance, whereas PREs are dependent on the sixth power. Furthermore, when looking at the prediction of the Ln ion position using PREs and PCSs and from plotting of calculated versus observed restraints it is evident that PCSs can be obtained with smaller errors. The measurement of chemical shifts is more precise and requires less signal-to-noise than the measurement of resonance intensities. Once the χ-tensor is available, these are clear advantages to choose PCS over PRE analysis when examining protein complexes. A fully rigid probe is a prerequisite for using PCSs over PREs.

Conclusions

This study indicates CLaNP-5 to be a broadly applicable paramagnetic probe. The size of its effects is dependent on the chelated metal and the direction of the paramagnetic effect is determined by the nature of the probe. Both features are independent of the local protein environment, yielding a priori predictable properties. Therefore, CLaNP-5 is an excellent tool to study the interactions of proteins in complexes with other small and large molecules.

Experimental Section

Materials. $Lu(OAc)_3$ was obtained from Acros (Geel, Belgium), other $Ln(OAc)_3$ were obtained from Sigma Aldrich (Zwijndrecht, The Netherlands), 1,4,7,10-tetraazacyclododecane-1,7-bis(*tert*-butyl acetate) was obtained from CheMatech (Dijon, France) and 2-(aminoethyl)methanethiosulfonate hydrobromide from Toronto Research Chemicals (North York, Canada). All other chemicals were reagent-grade commercial products and were used without further purification. Reactions were followed by TLC analysis on silica gel (F 1500 LS 254 Schleicher and Schuell, Dassel, Germany) or HPTLC aluminum sheets (silica gel 60, F254, Merck, Darmstadt, Germany), with detection by UV-absorption (254 nm). A Biocad Vision HPLC (PerSeptive Biosystems, Foster City, CA) and an Äkta basic FPLC (GE Healthcare Inc. Brussels, Benelux) were used for purifications. Analytical, semipreparative, and preparative reversed phase C18 columns were from obtained from Phenomenex (Torrance, CA), CM sepharose, HiTrap SP, and Superdex 75 columns were obtained from GE Healthcare. Silica gel (40−63 μm) was obtained from Fluka (Sigma Aldrich, Zwijndrecht, The Netherlands). Mass spectrometry was performed using a Finnigan (Thermo Fisher Scientific, Waltham, MA) LCQ LCMS system and a Finnigan LTQ Orbitrap system was used for HRMS and protein conjugation analysis. NMR was performed on a Bruker (Wormer, The Netherlands) AV 400 (400.23 MHz) and a Bruker Avance DMX 600 equipped with a TCI-Z-GRAD cryoprobe (600.1328 MHz). FTIR was performed on a Perkin-Elmer (Shelton, CT) Paragon 1000 FTIR spectrometer. Melting points were obtained using an SMP3 scientific melting apparatus (Stuart, Bibby Sterlin Ltd., Glamorgan, Wales).

Synthesis. 2-(Hydroxymethyl)pyridine-*N*-oxide (2). Following literature procedures,[44] 2-(hydroxymethyl)pyridine (5 g, 46 mmol) was dissolved in chloroform (75 mL) at 0 °C and treated with *meta*-chloroperbenzoic acid (13.5 g, 55 mmol). The mixture was allowed to warm to room temperature and stirring was continued for 18 h. Paraformaldehyde (1 g) was added to quench residual *meta*-chloroperbenzoic acid and stirred for 2 h. Ammonia was gently bubbled through the reaction mixture for 10 min, and the resulting slurry was dried with $MgSO_4$. The residue was applied to a continuous extraction cartridge and washed with dichloromethane (100 mL). Subsequently, the solid residue was extracted continuously with dichloromethane for 27 h. The combined organic layers were concentrated under reduced pressure and the residue was purified using silica gel column chromatography (methanol/dichloromethane/acetic acid, 4:95.5:0.5), giving 5.6 g (98%) of 2-(hydroxymethyl)pyridine-*N*-oxide as white needles. ^{1}H NMR (400 MHz $CDCl_3$): 4.82 (s, 2H), 7.28 (t, 1H), 7.35 (t, 1H), 7.40 (d, 1H), 8.25 (d, 1H). ^{13}C NMR (400 MHz $CDCl_3$): 61.7, 125.0, 125.1, 127.4, 139.8. HR-MS: *m*/*z* 126.05425 $[M + H]^+$, calcd $[C_6H_8NO_2]$ 126.05549. mp: 131 °C. FTIR: 3086.4, 2827.3, 1485.2, 1435.8, 1350.3, 1279.1, 1212.2, 1104.4, 1064.9, 840.1, 748.4, 692.5, 610.1, 447.9.

2-(Chloromethyl)pyridine-*N*-oxide (3). Adapted from literature procedures,[45] 2-(hydroxymethyl)pyridine-*N*-oxide (3.1 g, 25 mmol) was dissolved in freshly dissolved dichloromethane (100 mL) at 0 °C. Thionylchloride (3.2 g, 28 mmol) was added dropwise over 1 h. The reaction mixture was heated under reflux for 1 h. Ethanol (1 mL) was added to quench surplus of thionylchloride. Solvents were evaporated and the residue was recrystallized from acetone, yielding 3.4 g (94%) product as pale yellow/white needles. ^{1}H NMR (400 MHz $CDCl_3$): 5.08 (s, 2H), 7.89 (t, 1H), 8.14 (d, 1H), 8.22 (t, 1H), 9.15 (d, 1H). ^{13}C NMR (400 MHz $CDCl_3$): 38.8, 127.3, 128.1, 139.9, 141.1. HR-MS: *m*/*z* 144.02029 $[M + H]^+$, calcd $[C_6H_7NOCl]$ 144.02161. mp: 109 °C. FTIR: 3077.4, 2965.1, 1937.9, 1534.7, 1490.3, 1431.6, 1452.3, 1190.0, 849.0, 772.9, 749.5, 683.4, 452.0, 353.8.

1,4,7,10-Tetraazacyclododecane-1,7-[di-(*N*-oxido-pyridine-2-yl)methyl]-4,10-bis(2-(acetylamino)ethylmethanesulfonothioate) (6). 1,4,7,10-Tetraazacyclododecane-1,7-bis(*tert*-butyl acetate) (**4**, 1 g, 2.5 mmol) was dissolved in acetonitrile (100 mL) together with 2-(chloromethyl)pyridine-*N*-oxide (0.9 g, 6 mmol) in the presence of K_2CO_3 (1 g, 7 mmol) and stirred for 18 h at 80 °C. The reaction mixture was extracted with dichloromethane (3 × 25 mL), dried over $MgSO_4$ dissolved in a mixture of dichloromethane and trifluoroacetic acid (10 mL, 1:3 v/v) and stirred for 3 h at room temperature. Reaction mixture was concentrated under reduced

(42) Tang, C.; Ghirlando, R.; Clore, G. M. *J. Am. Chem. Soc.* **2008**, *130*, 4048–4056.
(43) Rumpel, S.; Becker, S.; Zweckstetter, M. *J. Biomol. NMR* **2008**, *40*, 1–13.
(44) Bremberg, U.; Rahm, F.; Moberg, C. *Tetrahedron: Asymmetry* **1998**, *9*, 3437–3443.
(45) Mizuno, Y.; Endo, T.; Miyaoka, T.; Ikeda, K. *J. Org. Chem.* **1974**, *39*, 1250–1255.

pressure and coevaporated with toluene. The crude mixture was dissolved in *N*,*N*-dimethylformamide (60 mL), triethylamine was added until the pH was neutral, 2-(aminoethyl)methanethiosulfonate hydrobromide (1.5 g, 6 mmol), *N*-hydroxysuccinimide (1.2 g, 10 mmol), and *N*-(3-dimethylaminopropyl)-*N*′-ethylcarbodiimide (1.9 g, 10 mmol) were added and stirred for 30 h at room temperature. The reaction mixture was concentrated under reduced pressure and purified by HPLC (0.1% trifluoroacetic acid and a 10−90% acetonitrile gradient on a C18 preparative column). Fractions containing product were pooled, concentrated, and freeze-dried; overall yield 1.6 g (84%) as a yellow oil. ^{1}H NMR (600 MHz D_2O, 348 K): δ 3.68 (s, 8H), 3.73−3.75 (m, 12H), 3.84 (s, 6H), 3.89 (s, 4H), 3.94 (t, 4H), 4.88 (s, 4H), 8.07 (t, 2H), 8.15 (t, 2H), 8.25 (d, 2H), 8.82 (d, 2H). ^{13}C NMR (600 MHz D_2O, 348 K): δ 35.1, 38.6, 49.7, 50.0, 50.2, 53.0, 55.0, 128.1, 129.8, 131.3, 140.2, the C═O was invisible in the APT spectrum. HR-MS: *m*/*z* 777.25557 $[M + H]^+$, calcd $[C_{30}H_{49}N_8O_8S_4]$ 777.25559. FTIR: 2933.4, 2362.5, 1666.4, 1389.5, 1317.6, 1129.6, 957.3, 706.9, 551.7.

Ln Ligation to 1,4,7,10-Tetraazacyclododecane-1,7-[di-(*N*-oxido-pyridine-2-yl)methyl]-4,10-bis(2-(acetylamino)ethylmethanesulfonothioate) (7a−f). A typical procedure is exemplified for the synthesis of Lu-CLaNP-5 (**7a**). $Lu(OAc)_3$ (9 mg, 20 μmol) was dissolved in *N*,*N*-dimethylformamide (0.2 mL). CLaNP-5 (**6**, 100 mg, 0.12 mmol) was disolved in *N*,*N*-dimethylformamide (0.5 mL). A total of 80 μL of the CLaNP-5 solution was added to the reaction mixture and stirred for 1 h at room temperature, giving quantitative yields. Ligation efficiency was monitored by LCMS (0.1% trifluoroacetic acid and a 10−90% acetonitrile gradient on a C18 analytical column), $[M + H]^+$ 949 *m*/*z*. ^{1}H NMR (600 MHz D_2O, 348 K): δ 3.19 (m, 8H), 3.49 (m, 8H), 3.601 (m, 8H), 3.81 (m, 4H), 3.91 (s, 6H), 4.41 (s, 4H), 8.25 (d, 2H), 8.32 (t, 2H), 8.43 (t, 2H), 9.00 (d, 2H). ^{13}C NMR (600 MHz D_2O, 348 K): δ 34.1, 39.0, 49.8, 52.8, 55.3, 55.9, 64.2, 128.0, 129.6, 136.5, 140.9, 145.5, 176.5. HR-MS: *m*/*z* 949.17334 $[M + H]^+$, calcd $[C_{30}H_{46}N_8O_8S_4Lu]$ 949.17291. FTIR: 3505.5, 2931.0, 2362.5, 1652.1, 1386.0, 1091.4, 658.2, 352.4, 321.1.The other Ln ions Yb, Eu, Dy, Gd, and Tm were chelated to **6** following the same procedure.

Lu-5 Complex. Lu was chelated to crude 1,4,7,10-tetraazacyclododecane-1,7-bis(acetate)-4,10-bis(pyridine-*N*-oxide) (**5**) similarly to described above and purified by HPLC. ^{1}H NMR (600 MHz D_2O, 350 K): δ 2.74 (s, 4H), 3.09−3.14 (m, 8H), 3.29 (s, 4H), 3.58 (s, 4H), 4.07 (s, 4H), 7.78 (d, 2H), 7.81 (t, 2H), 7.96 (t, 2H), 8.56 (d, 2H). ^{13}C NMR (600 MHz D_2O, 350 K): δ 54.2, 57.1, 57.2, 68.2, 129.0, 130.4, 137.6, 142.4, 146.8, 180.3. Large linewidths were found for the resonances of the protons of the polyaza-ring and the protons of the pyridine methylene groups. These resonances could only be resolved at elevated temperatures (348 K), indicating the cyclen ring to be in exchange between different conformational species. The methylene protons of the acetate pendant arms were well resolved.

Production Pseudoazurin Double Cys Mutants. The production and purification of the ^{15}N enriched *Alcaligenes faecalis* pseudoazurin (Paz) double cysteine mutant E51C/E54C was performed as described before,[19] with small modifications. Paz was purified on a CM column followed by a HiTrap SP column. Double cysteine mutations L8C/K10C and D100C/S104C were introduced in the pET24c vector, containing the Paz gene as a Nhe I and Xho I insert as described for the E51C/E54C mutant.[18] Forward and backward primers for L8C/K10C and D100C/S104C, respectively, were CATATGGCTAGCGAAAATATCGAAGTTCATATGTGC and the T7 reverse primer and GCCCGGCCAATCTATGCCA-GATCGTTTGCGCCAAGA and CGATCTGGTCTAGATTGGC-CGGG. Mutagenesis was confirmed by DNA sequencing. The expression and purification of these mutants were performed the same way as for the E51C/E54C mutant. All three mutants could be produced with yields varying between 5 and 50 mg/L.

Attachment of Probe to Protein (8a−j). To a 0.5 mM solution of Paz double cysteine mutant in 20 mM sodium phosphate pH 7.0 was added 5 mM dithiotreitol and incubated on ice for 1 h to reduce the cysteines. After washing away the surplus of dithiotreitol, 10 equiv of Ln-CLaNP-5 (**7a−f**) were added to a 60 μM solution of the reduced Paz in degassed buffer containing 20 mM sodium phosphate pH 7.0 supplemented with 150 mM NaCl and stirred on ice for 1 h under an argon atmosphere. Monomeric probe attached protein was purified from dimer and surplus of probe using a Superdex 75 column. In the case of Paz L8C/K10C an additional purification was performed on a HiTrap SP column. Probe attachment was in general >90% estimated from the absence of diamagnetic peaks in the [^{15}N, ^{1}H]-HSQC spectra. In the case of Yb-CLaNP-5 attached to ^{15}N-enriched Paz D100C/S104C, probe attachment was less efficient (60%), and clear diamagnetic peaks were visible in the spectrum. PCSs and RDCs could still be determined, however. The probe labeling efficiency was followed by mass spectrometry analysis. DTT treatment of ^{14}N Paz D100C/S104C (theoretical mass 13528.76 Da) reduced the mass from 14170.13 to 13528.02 Da, suggesting a loss of two glutathion- and two oxygen-adducts. Incubation of reduced Paz with Yb-CLaNP-5 yielded a mass of 14314.19 Da, indicating the probe to be attached via both pendant arms (theoretical mass 14314.62).

Fluorescence. Fluorescence of Eu-CLaNP-5 was measured in water on a Varian Cary Eclipse spectrometer. Fluorescence decay was recorded using excitation at a wavelength of 250 nm and measuring emission at 617 nm with bandwidths of 5 nm. Decay curves were fitted with a single exponential function in OriginPro 7.5 (www.OriginLab.com).

Protein NMR. Typically, NMR samples contained 100−500 μM Ln-CLaNP-5 attached Paz in 20 mM sodium phosphate, pH 7.0, 6% D_2O (v/v), and 1 equiv of ascorbic acid under an argon atmosphere to keep the Cu atom in the reduced state. [^{15}N, ^{1}H]-HSQC and IPAP spectra were recorded at 293 K on a Bruker Avance DMX 600 spectrometer equipped with a TCI-Z-GRAD cryoprobe. Data were processed in Azara (www.bio.cam.ac.uk/azara) and analyzed in Ansig for Windows.[46] The assignments of the resonances were based on previous work.[47] The fits of observed versus back-calculated NMR parameters are expressed in a quality factor Q, defined as the ratio of the rmsd between observed and calculated data and the rms of the observed.[48]

PCS-Based χ-Tensor Determinations. PCSs are defined as the difference in ppm between the resonances of a nucleus in a paramagnetic sample and a diamagnetic sample. Eu, Yb, Dy, and Tm containing CLaNP-5 are anisotropic paramagnetic probes and Lu-CLaNP-5 served as the diamagnetic sample. PCS is related to the distance between a nucleus and the paramagnetic ion according to eq 1

$$\mathrm{PCS} = \frac{1}{12\pi r^3}\left[\Delta\chi_{\mathrm{ax}}(3\cos^2\theta - 1) + \frac{3}{2}\Delta\chi_{\mathrm{rh}}(\sin^2\theta\cos 2\Omega)\right] \quad (1)$$

where r, θ, and Ω are the polar coordinates of the nucleus with respect to the principle axes of the χ-tensor and $\Delta\chi_{ax}$ and $\Delta\chi_{rh}$ are the axial and rhombic components of the χ-tensor, respectively. The structure of Paz was taken from PDB entry 1PY0 and the metal position was optimized by using X-PLOR-NIH version 2.9.9[49] and the XPCS energy term for PCS.[50] The χ-tensors were obtained by Euler rotation of Ln-centered Paz and fitting of the experimentally obtained PCSs to eq 1 as described.[51] The previously reported values for $\Delta\chi_{ax}$ and $\Delta\chi_{rh}$ of Yb-CLaNP-5 were in the wrong units.[29] The currently reported values should be used instead.

(46) Helgstrand, M.; Kraulis, P.; Allard, P.; Hard, T. *J. Biomol. NMR* **2000**, *18*, 329–336.
(47) Impagliazzo, A.; Ubbink, M. *J. Biomol. NMR* **2004**, *29*, 541–542.
(48) Hulsker, R.; Baranova, M. V.; Bullerjahn, G. S.; Ubbink, M. *J. Am. Chem. Soc.* **2008**, *130*, 1985–1991.
(49) Schwieters, C. D.; Kuszewski, J. J.; Tjandra, N.; Clore, G. M. *J. Magn. Reson.* **2003**, *160*, 65–73.
(50) Banci, L.; Bertini, I.; Cavallaro, G.; Giachetti, A.; Luchinat, C.; Parigi, G. *J. Biomol. NMR* **2004**, *28*, 249–261.
(51) Worrall, J. A.; Kolczak, U.; Canters, G. W.; Ubbink, M. *Biochemistry* **2001**, *40*, 7069–7076.

PRE-Based Gd Position Determination. From the intensity ratio (I_{para}/I_{dia}) of the amide resonances in the [^{15}N, ^{1}H]-HSQC spectra of Gd-CLaNP-5 attached Paz (para) and Lu-CLaNP-5 attached Paz (dia) the paramagnetic contribution to the ^{1}H T_2 relaxation can be extracted using eq 2.[6,19] The contribution of ^{15}N transversal relaxation is assumed negligible.

$$\frac{I^{\text{para}}}{I^{\text{dia}}} = \frac{R_2^{\text{dia}} \exp(-R_2^{\text{para}} t)}{R_2^{\text{dia}} + R_2^{\text{para}}} \tag{2}$$

where R_2^{dia} and R_2^{para} are, respectively, the diamagnetic and paramagnetic contribution to the transversal relaxation rate and t is the INEPT evolution time (9 ms). R_2^{dia} is obtained from the resonances linewidths ($\Delta\nu_{1/2}$) in the diamagnetic sample ($R_2^{\text{dia}} = \pi\Delta\nu_{1/2}$), as determined using Mestrec (www.mestrec.com). The intensity ratios were normalized using the resonances for residue 11, which according to the crystallized structure of CLaNP-1 bound Paz E51C/E54C (PDB entry 1PY0) is at 37 Å the farthest from the Ln ion and should not be sensitive to any relaxation effects caused by the Gd-ion. From the R_2^{para} the Gd ion to amide distances (r) were calculated using the simplified Solomon and Bloembergen equation, shown in eq 2[52]

$$r = \sqrt[6]{\frac{1}{15}\left(\frac{\mu_0}{4\pi}\right)^2 \frac{\gamma_H^2 g^2 \mu_B^2 J(J+1)}{R_2^{\text{para}}}\left(4\tau_c + \frac{3\tau_c}{1+\omega_H^2\tau_c^2}\right)} \tag{3}$$

where μ_0 is the permeability of vacuum, γ_H is the proton gyromagnetic ratio, μ_B is the Bohr magneton, g is the electronic g factor, J is the Gd quantum number (7/2), τ_c is the total correlation time (estimated to be 6.0 ns, based on fitting experimentally determined distances with PCS-derived distances), and ω_H is the Larmor proton spin frequency. For 75 amides the resonances were assigned and sufficiently resolved to yield reliable PREs. The obtained PREs were divided in three classes of restraints. The first class (20 restraints) contained those amide resonances for which the intensity ratio was less than 0.20. These residues are considered to be too close to Gd for accurate distance determination and to this class an upper limit of 20 (+4, −15) Å was assigned. The second class (43 restraints) was formed by the amide resonances with an intensity ratio between 0.20 and 0.83. For these residues the distances as determined from eq 3 were used. The third class (12 restraints) consisted of the amide resonances with an intensity ratio of more than 0.83. These residues are considered to be too far from Gd for accurate distance determination and to these were assigned a lower distance limit of 31 (−4, +100) Å. The three classes of restraints were used to model the position of the Gd-ion relative to the protein, by using restrained energy minimization in the program X-PLOR-NIH. The position of Gd was optimized while keeping the protein fixed (PDB entry 1PY0[18]).

RDC Analysis. RDCs caused by partial alignment of Paz in the magnetic field were quantified from in-phase antiphase (IPAP) spectra,[53] by subtracting the ^{15}N splittings of the paramagnetic samples of the diamagnetic sample. The RDCs were used to optimize the X-ray structure of Paz (PDB entry 1PY0) in X-PLOR-NIH, using the XRDC term for RDC restraints,[50] and the PCS-based $\Delta\chi_{ax}$ and $\Delta\chi_{rh}$. All the RDC data sets, obtained using Yb, Eu, Tm, and Dy for the E51C/E54C mutant, Yb for the L8C/K10C mutant, and Yb for the D100C/S104C mutant of Paz, were combined in a single optimization of the protein structure. An energy minimization was performed for 100 cycles without restraints, followed by 1000 cycles including the RDCs as restraints. Convergence was reached as indicated by a stable energy of the system. The rmsd of backbone atoms was 0.521 Å and that of the HN atoms 0.634 Å. With the obtained structure, the RDCs were backcalculated using eq 4[53,54]

$$D^{\text{res}} = -\frac{B_0^2}{15kT}\frac{\gamma_i\gamma_j h}{16\pi^3 r_{ij}^3}\left(\Delta\chi_{ax}(3\cos^2\theta - 1) + \frac{3}{2}\Delta\chi_{rh}\sin^2\theta\cos 2\phi\right) \tag{4}$$

where B_0 is the applied magnetic field, γ_i and γ_j are the gyromagnetic ratios of nuclei i and j, respectively, r is the $i-j$ internuclear distance (1.02 Å), θ and Ω determine the internuclear vector orientation with respect to the principle axes of the χ-tensor, and $\Delta\chi_{ax}$ and $\Delta\chi_{rh}$ are the axial and rhombic components of the χ-tensor, respectively. The χ-tensor parameters were subsequently determined using the optimized protein structure, the experimental data sets, and the computer software Module.[55] From the unitless axial χ-tensor value A_a, the corresponding $\Delta\chi_{ax}$ (10^{-32} m^3) was calculated using eq 5.

$$\Delta\chi_{ax} = A_a\frac{15\mu_0 kT}{B_0^2} \tag{5}$$

In analogy, the $\Delta\chi_{rh}$ was calculated from A_r. The previously reported values for $\Delta\chi_{ax}$ and $\Delta\chi_{rh}$ of Yb-CLaNP-5 were given in the wrong units.[29] The currently reported values should be used instead.

Prediction of χ-Tensors and their Effects. The position and direction of the χ-tensor of Yb-CLaNP-5 (**7b**) on Paz were predicted in X-PLOR-NIH using the X-ray structure of Paz (PDB entry 1PY0). The center of the χ-tensor, representing the Ln ion was placed at 8 Å from the Cα atoms of the residues to which CLaNP-5 is attached and 6 Å from all other atoms. The χ-tensor was oriented such that the x-axis makes a 20° angle with the vector between the Cα atoms of the CLaNP-5-attaching residues. The z-axis was placed parallel to the average direction of the Cα to Xγ atoms of the two CLaNP-5-attaching residues. With the predicted position and direction of the χ-tensor, PCSs were predicted using eq 1. A script for placing the χ-tensor pseudoatoms is provided in the Supporting Information.

Acknowledgment. We thank Dr. Miguel Prûdencio for help in mutagenesis, Dr. Rainer Wechselberger and the NMR facility of the Bijvoet Center in Utrecht for use of the 900 MHz spectrometer, and Hans van der Elst for assistance with all MS measurements. The Volkswagenstiftung supported this work, Grant No. I/80 854.

Supporting Information Available: Figures S1−S6, containing the fits of PRE-based to PCS-based amide-to-Ln ion distances, the fits of observed-to-calculated PCSs and RDCs and PREs and PCSs plotted per residue, and the script to predict PCS on a given protein structure. This material is available free of charge via the Internet at http://pubs.acs.org.

JA8054832

(52) Solomon, I.; Bloembergen, N. *J. Chem. Phys.* **1956**, *25*, 261–266.
(53) Tjandra, N.; Omichinski, J. G.; Gronenborn, A. M.; Clore, G. M.; Bax, A. *Nat. Struct. Biol.* **1997**, *4*, 732–738.
(54) Valafar, H.; Prestegard, J. H. *J. Magn. Reson.* **2004**, *167*, 228–241.
(55) Dosset, P.; Hus, J. C.; Marion, D.; Blackledge, M. *J. Biomol. NMR* **2001**, *20*, 223–231.